Synthesis and Characterization of Aligned ZnO Nanorods on Porous Aluminum Oxide Template

Jiansheng Jie,[†,‡] Guanzhong Wang,*[,†,‡] Qingtao Wang,[†,‡] Yiming Chen,[†,‡] Xinhai Han,[†,‡] Xiaoping Wang,[†,‡] and J. G. Hou[†]

Hefei National Laboratory for Physical Sciences at Microscale, and Department of Physics, University of Science and Technology of China, Hefei 230026, China

Received: March 7, 2004; In Final Form: June 9, 2004

Aligned high-density ZnO nanorods were successfully synthesized on porous aluminum oxide (PAO) template. The growth process involves carbonthermal reduction of ZnO as a Zn vapor source and ZnO nucleation on the PAO template without metal catalysts. Field-emission scanning electron microscope images revealed that the nanorods have uniform length distributions and hexagon end planes, and the intense *c*-axis growth was also confirmed by X-ray diffraction. Strong ultraviolet emission at 380 nm and weak green band emission at 520 nm at room-temperature photoluminescence clearly indicated the high quality of the ZnO nanorods. A growth mechanism is proposed that the multipore surface of the PAO template plays a critical role in the nucleation of ZnO in the initial stage of growth, and nanorods grow from the nuclei due to intense ZnO *c*-axis orientation growth.

Introduction

One-dimensional (1D) semiconductor nanowires have attracted much attention due to their novel properties which make them potentially ideal functional components for nanometer-scale electronics and optoelectronics.[1−3] In the past decade, there have been many research papers on the synthesis of various 1D semiconductor nanostructures.[4−6] Recently, great efforts have been placed on the fabrication of nano-devices using these 1D semiconductor nanostructures.[7−9] Among these semiconductor systems, oxide semiconductors have attracted special interest for their unique optical and electric properties.[10] An obvious advantage is the properties of oxide semiconductors can be easily controlled through altering the concentration of oxygen vacancies in them. Among them, ZnO is a wide direct band-gap (3.37 eV) oxide semiconductor that is regarded as a promising ultraviolet optoelectronic material. An outstanding feature of ZnO is the large exciton binding energy (60 meV) as compared with that of conventional semiconductors, such as Si (14.7 meV), ZnS (37 meV), and GaN (25 meV), which enables the laser operating at room temperature with low threshold.[11] ZnO optically pumped laser emission has been reported in disordered particles, thin fims, and recently in a ZnO nanowire array and single ZnO nanoribbon.[12−14]

Application of semiconductor nanostructures in devices is the focus of recent nanoscience research. For this purpose, nanostructures with controlled crystalline morphology, orientation, and surface architectures are needed. However, it still remains a significant challenge to obtain controllable growth of well-ordered nano-arrays. Among ZnO nanostructures, oriented ZnO nanowires are highly interesting for their great potential application in laser emission, gas sensor, and field emission devices. Using the gas-phase evaporation method, Huang et al.[11] have successfully synthesized aligned ZnO nanowires on Au pattern-coated sapphire (110) substrate. Park et al.[15] also prepared aligned ZnO nanorods on sapphire (001) substrate using the metallorganic vapor-phase epitaxial growth method. Recently, Tseng et al.[16] demonstrated that needlelike ZnO nanowires with high density and a growth direction perpendicular to the Ga-doped ZnO substrate could be synthesized through vaporizing the Zn metal powder directly at low temperature. Electrical alignment of ZnO nanorods was also reported by Weller et al.[17]

Here, we demonstrate another effective approach to prepare high-quality ZnO nanorods with high density and well order. Aligned ZnO nanorods were synthesized on the surface of porous aluminum oxide (PAO) template using carbonthermal reduction of ZnO as a zinc vapor source and air as the oxygen source. As compared with previous reports, the method used in this research is very simple and of low cost because no metal catalyst or special substrate is needed. In addition, the roots of nanorods stick together and form a thick merged layer on the substrate, which can serve as an excellent conducting layer. Thus, the insulating substrate (PAO template is an insulator) will not bring unfavorable influence in the electrical device applications of the nanorods, such as in field emission displays. It can be expected that the aligned ZnO nanorods should be very useful for many device applications.[18]

Experimental Section

A horizontal tube furnace was used as the evaporation apparatus. The source material, ZnO (99.99% pure) powder mixed with graphite powder (molar ratio 1:1), was placed in the closed end of a quartz tube ($\Phi 1 \times 25$ cm). A piece of PAO template (through-hole thickness and pore diameter were 25 μm and 60−100 nm, respectively) was then placed into the tube at a distance of about 8 cm away from the evaporation source. The quartz tube was then inserted into the tube furnace and heated to 1150 °C and maintained at this temperature for 10 min. Meanwhile, a dry air flow was introduced through the tube

* Corresponding author. Phone: +86-551-3600075. Fax: +86-551-3603323. E-mail: gzwang@ustc.edu.cn.
† Hefei National Laboratory for Physical Sciences at Microscale.
‡ Department of Physics.

10.1021/jp048974r CCC: $27.50
Published on Web 07/21/2004

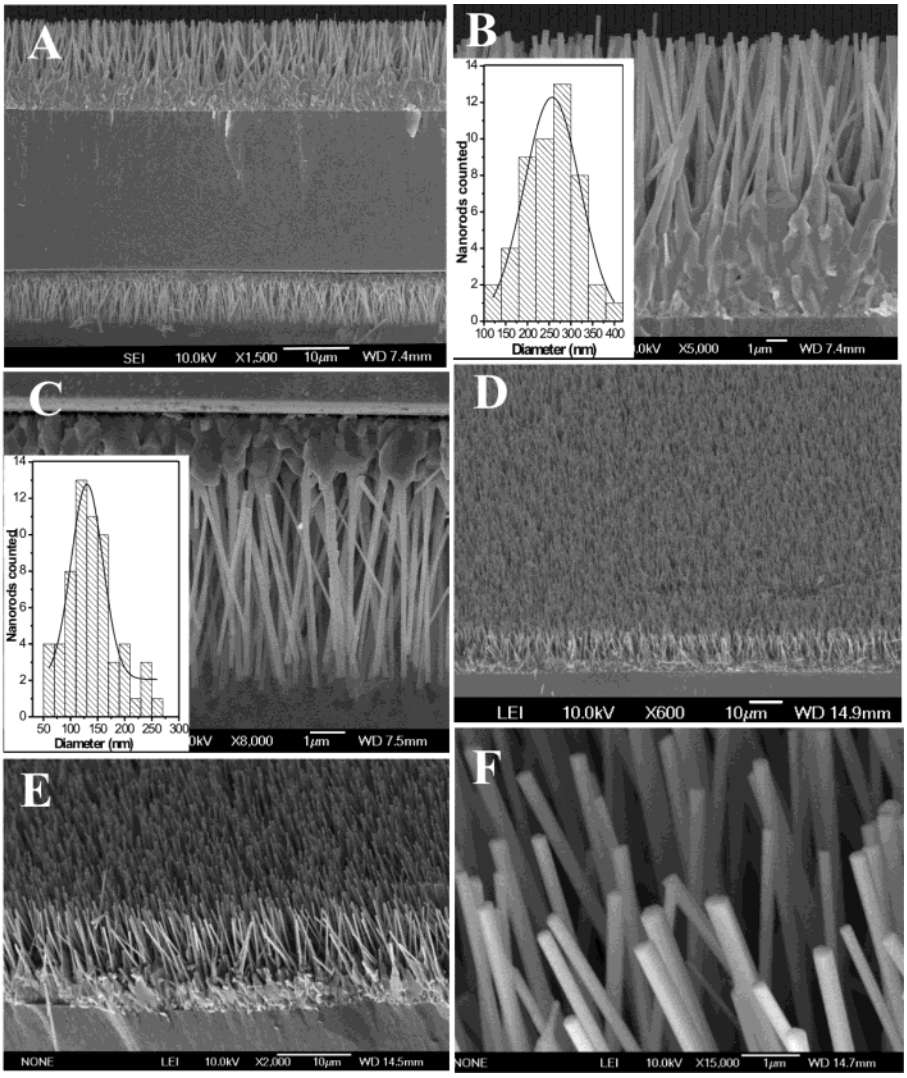

Figure 1. (A) FE-SEM image of the cross section of alumina template; ZnO nanorods grew on both up- and down-surfaces of the template. (B), (C) show enlarged images of the ZnO array on up- and down-surfaces of the template, respectively. Insets show the histograms of ZnO nanorods diameters. The smooth curves show a Gaussian fit of the rod diameter distribution. (D) Tilted view of the ZnO array on the up-surface. (E) Tilted view of the ZnO array, with larger magnification. (F) Enlarged image of the ends of the nanorods on the up-surface.

furnace at a flow rate of 150 standard cubic centimeters per minute (sccm), and the pressure in the tube was finally adjusted to about 80 Torr. The temperature of the PAO template was in the range of 700−900 °C during the experiment. After the reaction was terminated and the furnace cooled to room temperature, the PAO template was taken out of the quartz tube and a layer of black product was found on the surface of the template. A field-emission scanning electron microscope (FE-SEM) (JEOL model JSM-6700F) was used to observe the morphology of the products. X-ray diffraction (XRD) (MAC Science, model MXPAHF) spectra of the prepared nanostructures were recorded using standard Cu Kα radiation. Further structural characterization was performed on a transmission electron microscope (TEM) (JEOL model 2010) operating at 200 kV. The room-temperature photoluminescence spectrum (RT-PL) was measured using a He−Cd laser (325 nm) as the excitation source.

Results and Discussion

The general morphology of as-prepared aligned ZnO nanorods was investigated using FE-SEM. Figure 1 displays the (A−C) cross-view and (D−F) tilted view images of the aligned ZnO nanorod array on the PAO template. From the FE-SEM images, it can be seen that aligned ZnO nanorods with high density were uniformly grown over the entire surface of the PAO template, including both the up- and the down-surfaces. Histograms of the nanorods diameters on the up- and down-surfaces are plotted in the insets of Figure 1B,C, respectively. The diameters of nanorods on up- and down-surfaces distribute in the ranges of 100−450 and 50−280 nm, respectively. The diameter dispersity is due to the inhomogeneous sizes of the initial ZnO nuclei, which should be discussed in the growth process. Furthermore, the diameters distributions are well fitted using Gaussian curves, and the average diameters of the nanorods on up- and down-surfaces are 260 and 130 nm, respectively. In addition, nanorods on the up-surface were longer than nanorods on the down-surface (∼14 μm vs 7.6 μm, the length is measured from the surface of template to the top end of the nanorod). These results must be caused by the slant of the template during the experiment, which makes the up-surface facing the vapor flow, and therefore nanorods on the up-surface have a higher growth rate than nanorods on the down-surface. However, it is an interesting phenomenon that the aspect ratios of nanorods on up- and down-surfaces are nearly equal (14 μm:260 nm ≈ 7.6 μm:130 nm), revealing the growth ratio of nanorods in the longitudinal direction and in the transverse direction might be

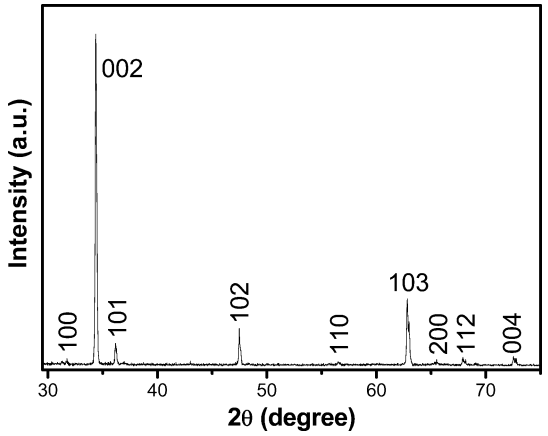

Figure 2. X-ray diffraction pattern of the as-prepared products.

independent from the concentrations of the reactants in the vapor. From the sectional view images, we can also confirm that the ZnO nanorods were grown from the columnar grains on the roots and the roots of the nanorods on the up-surface were closely stuck together to form a bulky crystalline layer. The end planes of the ZnO nanorods are smooth and have hexagonal or near hexagonal shapes [see Figure 1F], corresponding to the ZnO (001) plane and revealing good crystal quality of the nanorods. It is noted that the pores of the template were entirely empty, confirmed by both the FE-SEM and the subsequent TEM investigations. These results reveal the nanorods were grown on the surface but not from the pores of the template.

The crystallographic properties of the nanorods were investigated by XRD. As shown in Figure 2, all of the diffraction peaks can be indexed by ZnO wurtzite structure with $a = 3.253$ Å and $c = 5.216$ Å, respectively, corresponding to the results of bulk ZnO. The ZnO (002) peak is the dominant peak, and its intensity is much higher than other peaks, revealing high (001) growth orientation of the ZnO nanorods. The weaker peaks, such as (101) and (102), are suggested as mainly coming from the thick merged layer on the roots of ZnO nanorods, which is composed of lots of crystal grains and shows a polycrystalline structure. Diffraction from the PAO template was not observed in the XRD pattern not only due to its amorphous structure but also due to the thick ZnO layer on it.

Further structure characterization of the ZnO nanorods was performed by TEM. Figure 3 shows the TEM image and the corresponding selected-area electron diffraction (SAED) pattern of the ZnO nanorod. These results confirmed that the ZnO nanorod was single crystal with uniform structure. The end plane of the rod is smooth, in accordance with the result of the SEM investigation. In addition, no metal catalyst was found on the top or bottom of the nanorods, implying a growth mechanism different from the conventional vapor−liquid−solid (VLS) growth mechanism,[19] in which nanosized metal particles are usually found on the ends of 1D nanostructures. From analysis of the SAED pattern, the growth direction of the nanorod could be confirmed along the ZnO [001] direction. This result is consistent with the SEM investigation and XRD measurement.

The optical properties of ZnO nanorods were investigated by PL spectroscopy. As shown in Figure 4, an intensive sharp peak at ~380 nm with the full width at half-maximum of 120 meV is the dominant peak in the room-temperature PL spectrum of ZnO nanorods. The UV emission is consistent with the results in previous reports and has been attributed to the near band-edge emission of ZnO.[20,21] In addition, a very weak green emission band near 520 nm is also observed. It is a deep-level

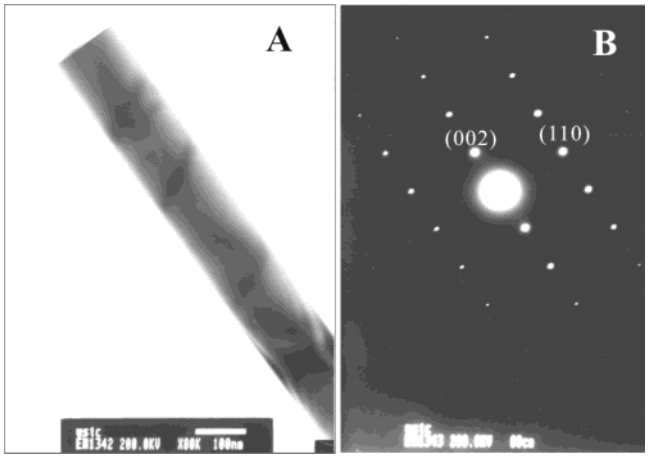

Figure 3. (A) TEM image of a single ZnO nanorod. (B) Corresponding ED pattern, revealing the nanorod is single crystal and grows along [001] orientation.

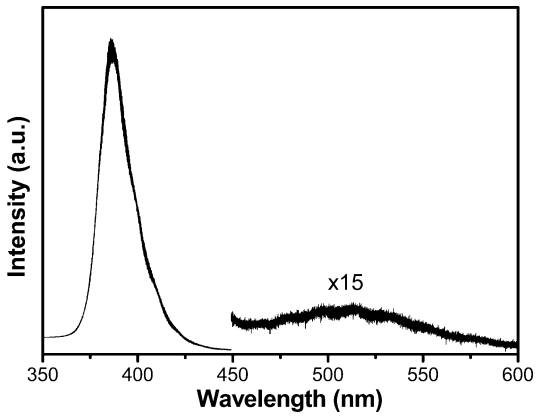

Figure 4. Room-temperature photoluminescence spectra of an as-prepared sample.

transition corresponding to singly ionized oxygen vacancy in ZnO and coming from the recombination of a photogenerated hole with the single ionized charge state of this defect.[22] The intensity of the deep-level emission is determined by the concentration of the oxygen vacancies in the ZnO crystal.[23] Therefore, the weak green band in the PL spectrum means that there is a low concentration of oxygen vacancies in the ZnO nanorods and reveals the high optical quality of the ZnO nanorods. For nanostructured semiconductors, quantum confinement effects are often expected and observed,[24,25] which usually induce the blue-shift of the emission peaks in the PL spectrum. However, no such phenomenon can be observed when comparing the PL spectrum of the ZnO nanorods with that of ZnO bulk. It is reasonable because the diameters of ZnO nanorods are far larger than the Bohr radius of ZnO (about 2 nm), thus causing the invalidation of quantum confinement effects in the ZnO nanorods.

For investigating the growth process of the aligned ZnO nanorods, we observed the morphologies of the sample when the growth time was only 15 s and the pressure of the reaction chamber was lower than 10 Torr and the flow rate of air was about 20 sccm. The FE-SEM images of the sample are shown in Figure 5. Dense and oriented ZnO nuclei, with sizes ranging from 15 to 40 nm, can be observed on the open ends of the pores of the PAO template, which clearly indicates the origin of the aligned ZnO nanorods.

On the basis of the analysis of the experimental results, a nucleation growth mechanism is proposed to interpret the growth of the ZnO nanorods, which is illustrated in Figure 6. The empty

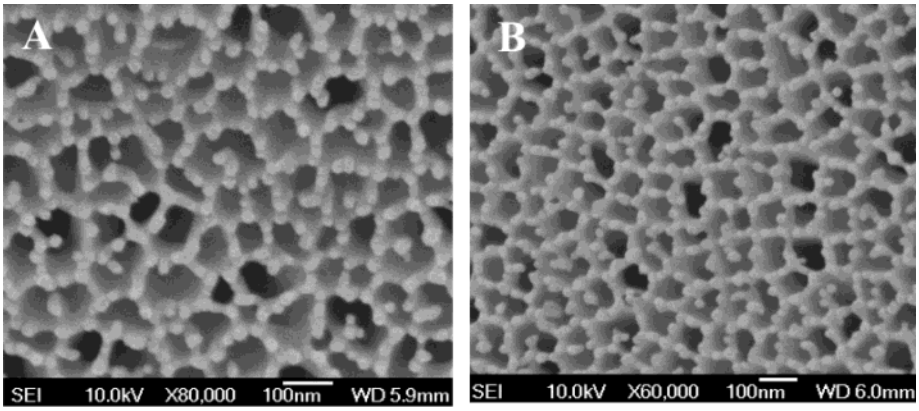

Figure 5. FE-SEM images of the sample with a growth time of 15 s; dense and orientated ZnO nuclei can be observed on the open ends of the pores of the PAO template.

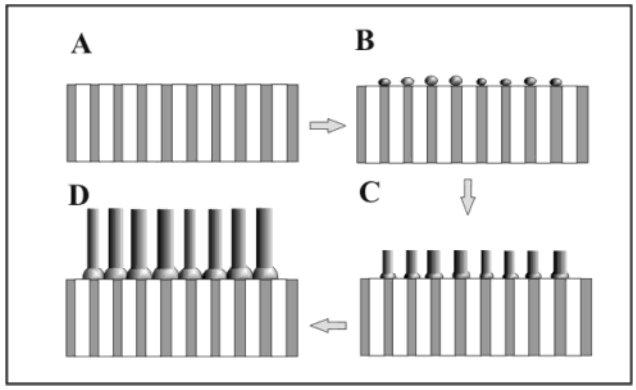

Figure 6. Schematic illustration of the growth process of the aligned ZnO nanorods on PAO template. (A) Empty PAO template at the beginning of reaction. (B) Nanosized Zn liquid droplets precipitated from the supersaturated Zn vapor and deposited onto the surface of PAO template. (C) While air was introduced into the tube furnace, Zn liquid droplets were oxidized and formed ZnO nuclei. (D) With the reaction going on, ZnO nanorods would grow from the ZnO nuclei because of the intense *c*-axis orientation growth.

PAO template, as shown in Figure 6A, has a number of pores with diameters 60−100 nm before the reactions. When the evaporation source is heated to a high temperature, carbon reduces ZnO into Zn vapor through carbonthermal reactions, and then the Zn vapor diffuses along the quartz to the lower-temperature zone where the PAO template is located. Liquid Zn droplets precipitate from the supersaturated Zn vapor and sediment onto the surface of PAO template [see Figure 6B]. Because of its multipore surface, PAO template is a very suitable substrate on which the high-density nanosized Zn liquid droplets can form. It can be expected that the Zn liquid droplets should assemble at the open ends of the pores. While air is introduced into the reaction chamber, nanosized Zn liquid droplets are oxidized and ZnO nuclei form on these sites [see Figure 6C]. For the growth of ZnO crystal, [001] has been demonstrated to be the preferred growth direction, and the growth rate along the *c*-axis is much faster than that along other crystal directions.[26,27] Therefore, the ZnO nuclei should have [001] orientation and nanosizes of which limited the initial sizes of the nanorods. With the reactions going on, more and more Zn vapor reaches the surface of PAO template, which sustains the growth of nanorods on the longitudinal and transverse directions [see Figure 6D]. It is expected that the sizes of the nanorods were determined by the growth time, pressure of oxygen in the chamber, and the concentration of Zn vapor. The diameter dispersivity of the nanorods is mainly due to the inhomogeneous sizes of the initial ZnO nuclei. In addition, ZnO nuclei would possibly merge together during the growth process and also induced the change of the sizes of the ZnO nanorods. The morphologies and growth mechanism of the aligned ZnO nanorods on PAO template are similar to those reported by Tseng et al.[16] In that experiment, ZnO nuclei were formed on Ga-doped ZnO films, and aligned needlelike ZnO nanowires grew from these nuclei subsequently.

It has been noted that there is a bulky crystalline phase in the bottom of ZnO nanorods. We suggest two reasons might be responsible for this phenomenon. First, as the growth time increased, the ZnO nanorods grew larger and their roots stuck together. Second, ZnO layers were also formed on the surface of the template and then filled the gap of the ZnO nanorods on the bottom, which also made the roots of the nanorods connect together. Based on the experimental results, the thickness of the bulky crystalline phase should be determined by the growth time and the concentration of the reaction vapor.

Conclusion

In conclusion, the growth of aligned ZnO nanorods on PAO template with high density was demonstrated. In the growth process, carbonthermal reduction of ZnO was used as a Zn vapor source, and no metal catalyst was involved. FE-SEM images revealed that the nanorods have uniform length distributions and their end planes are hexagonal. Furthermore, XRD demonstrated the intense *c*-axis growth of the nanorods. Strong ultraviolet emission at ∼380 nm and weak green band emission at 520 nm in the room-temperature PL measurement gave a clear indication of the high quality of the ZnO nanorods. A possible growth mechanism was proposed. In this mechanism, the multipore surface of PAO template plays the critical role in the nucleation of ZnO in the initial stage, and then the nanorods grew from the ZnO nuclei because of intense *c*-axis orientation growth. It is reasonable to expect that aligned ZnO nanorods prepared by this approach can be very useful in device applications.

Acknowledgment. We thank Professor S. Y. Zhang, Mr. G. P. Li, and Prof. F. Q. Li for their assistance in the SEM and TEM experiments. This work was supported by the Natural Science Foundation of China (Grant Nos. 60376008, 50121202).

References and Notes

(1) Gudiksen, M. S.; Lauhon, L. J.; Wang, J. F.; Smith, D. C.; Lieber, C. M. *Nature* **2002**, *415*, 617.

(2) Park, W. I.; Jun, Y. H.; Jung, S. W.; Yi, G. C. *Appl. Phys. Lett.* **2003**, *82*, 964.

(3) Duan, X.; Huang, Y.; Agarwal, R.; Lieber, C. M. *Nature* **2003**, *421*, 241.
(4) Morales, A. M.; Lieber, C. M. *Science* **1998**, *279*, 208.
(5) Yang, P.; Wu, Y.; Fan, R. *Int. J. Nanosci.* **2002**, *1*, 1−39.
(6) Xia, Y.; Yang, P.; Sun, Y.; Wu, Y.; Mayers, B.; Gates, B.; Yin, Y.; Kim, F.; Yan, H. *Adv. Mater.* **2003**, *15*, 253.
(7) Cui, Y.; Lieber, C. M. *Science* **2001**, *291*, 851.
(8) Cui, Y.; Wei, Q.; Park, H.; Lieber, C. M. *Science* **2001**, *293*, 1289.
(9) Wang, Z. L. *Adv. Mater.* **2003**, *15*, 432.
(10) Pan, Z. W.; Dai, Z. R.; Wang, Z. L. *Science* **2001**, *291*, 1947.
(11) Huang, M. H.; Mao, S.; Feick, H.; Yan, H.; Wu, Y.; Kind, H.; Weber, E.; Russo, R.; Yang, P. D. *Science* **2001**, *292*, 1897.
(12) Mitra, A.; Thareja, R. K. *J. Appl. Phys.* **2001**, *89*, 2025.
(13) Sternschulte, H.; Thonke, K.; Sauer, R.; Koizumi, S. *Phys. Rev. B* **1999**, *59*, 12924.
(14) Yan, H.; Johnson, J.; Law, M.; He, R.; Knutsen, K.; Mckinney, J. R.; Pham, J.; Saykally, R.; Yang, P. *Adv. Mater.* **2003**, *22*, 1907.
(15) Park, W. I.; Kim, D. H.; Jung, S.-W.; Yi, G.-C. *Appl. Phys. Lett.* **2002**, *80*, 4232.
(16) Tseng, Y.-K.; Huang, C.-J.; Cheng, H.-M.; Lin, I.-N.; Liu, K.-S.; Chen, I.-C. *Adv. Funct. Mater.* **2003**, *13*, 811.
(17) Harnack, O.; Pacholski, C.; Weller, H.; Yasuda, A.; Wessels, J. M. *Nano Lett.* **2003**, *3*, 1097.
(18) Fan, S.; Chapline, M. G.; Franklin, N. R.; Tombler, T. W.; Cassell, A. M.; Dai, H. *Science* **1999**, *283*, 512.
(19) Duan, X.; Lieber, C. M. *Adv. Mater.* **2000**, *12*, 298.
(20) Xing, Y. J.; Xi, Z. H.; Xue, Z. Q.; Zhang, X. D.; Song, J. H.; Wang, R. M.; Xu, J.; Song, Y.; Zhang, S. L.; Yu, D. P. *Appl. Phys. Lett.* **2003**, *83*, 1689.
(21) Li, Y. B.; Bando, Y.; Sato, T.; Kurashima, K. *Appl. Phys. Lett.* **2002**, *81*, 144.
(22) Vanheusden, K.; Warren, W. L.; Seager, C. H.; Tallant, D. R.; Voigt, J. A.; Gnade, B. E. *J. Appl. Phys.* **1996**, *79*, 7983.
(23) Huang, M. H.; Wu, Y.; Feick, H.; Tran, N.; Weber, E.; Yang, P. *Adv. Mater.* **2001**, *13*, 113.
(24) Par, W. I.; Yi, G.-C.; Kim, M.; Pennycook, S. J. *Adv. Mater.* **2003**, *15*, 526.
(25) Li, B. B.; Yu, D. P.; Zhang, S. L. *Phys. Rev. B* **1999**, *59*, 1645.
(26) Laudise, R. A.; Kolb, E. D.; Caporaso, A. J. *J. Am. Ceram. Soc.* **1964**, *47*, 9.
(27) Li, W.-J.; Shi, E.-W.; Zhong, W.-Z.; Yin, Z.-W. *J. Cryst. Growth* **1999**, *203*, 186.